the two major clades of avian evolution, the Sauriurae and the Ornithurae, were sympatric only a few million years after the occurrence of *Archaeopteryx*. By the Jurassic-Cretaceous transition, birds had already undergone a remarkable and probably rapid radiation. The new information on the early geographic and temporal distribution of birds may also indicate a long avian history in the Jurassic. We would expect that the common ancestor of the Sauriurae and the Ornithurae would predate *Archaeopteryx* and that we may reasonably search for birds in Middle Jurassic and older beds. This exacerbates one of the most obvious conundrums facing the theory of a dinosaurian origin of birds. The dinosaurs thought to be most like birds are primarily Late Cretaceous in age and are younger than *Archaeopteryx* by more than 76 million years. This temporal paradox has led some dinosaur experts to argue that birds gave rise to certain late Cretaceous theropods (*23*).

The dating of the Jurassic-Cretaceous boundary remains controversial in northeastern China (*8*). We have accepted an age for *Confuciusornis* and *Liaoningornis* somewhat younger than *Archaeopteryx* but still older than any other known birds, and we think that these deposits essentially bridge the Jurassic-Cretaceous transition. Any more precise dating will require further field work in China.

REFERENCES AND NOTES

1. L. M. Chiappe, *Nature* **378**, 349 (1995).
2. L. D. Martin, *Cour. Forschungsinst. Senckenb.* **181**, 25 (1995); C. A. Walker, *Nature* **292**, 51 (1981).
3. A. Feduccia, *Science* **267**, 637 (1995).
4. E. N. Kurochkin, *Cretaceous Res.* **6**, 272 (1985).
5. L. Hou, *Sci. Sin. Ser. B* **27**, 1296 (1984).
6. L. Hou and J. Zhang, *Vertebr. Palasiat.* **31**, 217 (1993).
7. L. D. Martin, in *Perspectives in Ornithology*, A. H. Brush and G. A. Clark Jr., Eds. (Cambridge Univ. Press, New York, 1983), pp. 291–338.
8. L. Hou, Z. Zhou, Y. Gu, H. Zhang, *Chin. Sci. Bull.* **40**, 1546 (1995); L. Hou, Z. Zhou, L. D. Martin, A. Feduccia, *Nature* **377**, 616 (1995).
9. L. Hou, *Chin. Sci. Bull.*, in press.
10. J. Ruben, personal communication.
11. A. Chinsamy, L. M. Chiappe, P. Dodson, *Nature* **368**, 196 (1994).
12. Z. Zhou, *Cour. Forschungsinst. Senckenb.* **181**, 9 (1995).
13. A. Elzanowski, *Nature* **264**, 51 (1976); *Palaeontol. Pol.* **42**, 147 (1981).
14. J. L. Sanz, J. F. Bonaparte, A. Lacasa, *Nature* **331**, 433 (1988); J. L. Sanz and A. D. Buscalioni, *Paleontology* **35**, 829 (1992); A. Lacasa, *Estud. Geol.* **45**, 417 (1989); J. L. Sanz, L. M. Chiappe, A. D. Buscalioni, *Am. Mus. Novit.* **3133**, 1 (1995); J. L. Sanz *et al.*, *Nature* **382**, 442 (1996).
15. L. M. Chiappe, *Am. Mus. Novit.* **3083**, 1 (1993).
16. Z. Dong, *Can. J. Earth Sci.* **30**, 2177 (1993).
17. P. C. Sereno and Rao Chenggang, *Science* **255**, 845 (1992).
18. Z. Zhou, F. Jin, J. Zhang, *Chin. Sci. Bull.* **37**, 1365 (1992).
19. Z. Zhou, *Vertebr. Palasiat.* **33**, 99 (1995).
20. The data matrix and PAUP analysis are available at *Science*'s Beyond the Printed Page site on the World Wide Web: http://www.sciencemag.org/science/feature/data/hou.shl
21. E. N. Kurochkin, special issue of the Palaeontological Institute of the Russian Academy of Sciences, Moscow (1996).
22. L. M. Chiappe, in *Contribution of South America to Vertebrate Paleontology*, G. Arratia, Ed., *Muenchener Geowiss. Abh.* **A30**, 203 (1996).
23. G. Paul, *Predatory Dinosaurs of the World* (Simon and Schuster, New York, 1988).

24. We thank J. Chorn and D. Miao for reading the manuscript, C. Bennett for helpful suggestions, and the Chinese Natural Science Foundation and the National Geographic Society (U.S.) for support for fieldwork. Zhang Jie and S. Whitfield kindly helped prepare the figures; the drawings are by M. Tanner and M. A. Klotz.

17 July 1996; accepted 24 September 1996

Direct Observation of Vortex Dynamics in Superconducting Films with Regular Arrays of Defects

K. Harada, O. Kamimura, H. Kasai, T. Matsuda, A. Tonomura, V. V. Moshchalkov

The microscopic mechanism of the matching effect in a superconductor, which manifested itself as the production of peaks or cusps in the critical current at specific values of the applied magnetic field, was investigated with Lorentz microscopy to allow direct observation of the behavior of vortices in a niobium thin film having a regular array of artificial defects. Vortices were observed to form regular and consequently rigid lattices at the matching magnetic field, at its multiples, and at its fractions. The dynamic observation furthermore revealed that vortices were most difficult to move at the matching field, whereas excess vortices moved easily.

Many efforts have been made to increase the critical current density J_c of superconductors by introducing defects as pinning centers into superconductors. A high J_c, the maximum current density at which these defects can still pin down vortices against the Lorentz force exerted on vortices by a current, can be obtained when the elementary pinning force of individual pinning centers is strong.

However, the pinning effect cannot be estimated without taking the whole behavior of vortices into consideration. In fact, J_c has peak values at specific applied magnetic fields H (*1*, *2*). This "matching effect" has been attributed to the commensurability between arrays of vortices and defects: J_c (*3*) and the magnetization M (*4–6*) measured for superconductors with a regular array of artificial defects had peaks or cusps at specific H values, or "matching fields" $H = H_n$. The H values corresponded to the cases where the occupation number n of vortices at defects was an integer or its fractions. Hence, indirectly, the increase in J_c was related to the formation of regular and rigid vortex lattices assisted by the existence of defects.

In the present experiment, the static and dynamic behaviors of individual vortices were directly observed in superconducting thin films with a square array of artificial defects, in order to elucidate the microscopic mechanism of the matching effect. The simultaneous static observation of both vortices and defects that is necessary for such experiments has been made only for special cases with Bitter techniques (*7–9*) and scanning probe microscopy (*10*, *11*). At the same time, Lorentz microscopy (*12*) and electron holography (*13*) using a 300-kV field emission electron microscope have opened a way for simultaneous observation of both vortices and defects, not only statically but also dynamically. This has made it feasible to investigate the dynamic interaction of vortices with pinning centers (*14*, *15*). The present experiment was carried out with Lorentz microscopy.

The experimental procedure was as follows. A Nb thin-film sample was prepared by chemically etching 15-μm-thick foil that had been annealed at 2200°C for 10 min to increase its grain sizes up to ~300 μm in diameter. The film had one or more holes in the central part: In peripheral regions in the film that were <100 nm thick near the holes, a square array of 13 by 13 small defects was produced inside a region 10 μm by 10 μm (defect spacing d = 0.83 μm) by irradiation of the Nb film with a focused 30-kV Ga^+ ion beam from a Hitachi focused ion beam machine (FB-2000). The defect consisted of a pit 30 nm in diameter and a few nanometers in depth, and of dislocation networks 200 nm in di-

K. Harada, O. Kamimura, H. Kasai, T. Matsuda, A. Tonomura, Advanced Research Laboratory, Hitachi, Ltd., Hatoyama, Saitama 350-03, Japan.
V. V. Moshchalkov, Laboratorium voor Vaste-Stoffysica en Magnetisme, Katholieke Universiteit Leuven, B-3001 Leuven, Belgium.

ameter surrounding the pit. The pit with the dislocation networks is simply called a "defect" hereafter. Such square defect regions were repeatedly produced side by side parallel to the film edge at intervals of 4 μm.

The sample was set on a low-temperature stage in the electron microscope so that the film was tilted at an angle of 45° both to the incident electron beam and to H. The vortices appeared as spots of bright and dark contrast in an out-of-focus plane as a Lorentz micrograph (*12*), because the parallel beam of incident electrons was slightly deflected when passing through a vortex. The out-of-focus distance was 20 to 30 mm and the image magnification was ~×1000.

First, the configuration of vortices was observed at various values of H to investigate what happens to vortices at specific magnetic fields. When H was applied to the sample at temperature T = 10 K (which was greater than critical temperature T_c) and the sample was then cooled down to T = 4.5 K, vortices moved for a few minutes as a result of the nonuniform film thickness until they reached an equilibrium state. Lorentz micrographs of vortices were then made. The vortex density changed a little bit from one place to another because of the change in thickness. For our observation, we chose the region where the film was ~100 nm thick and the vortex density showed no appreciable change.

The observation revealed that vortices formed regular configurations at the matching magnetic fields H_n (components perpendicular to the film plane), which are given by $H_n = n \times \Phi_0/d^2 = n \times 29.8$ G, where Φ_0 is the quantized flux of a vortex.

Lorentz micrographs were taken at various matching fields (Fig. 1). In the case of $H_{1/4}$ (Fig. 1A), horizontal lines of vortices occurred at every fourth pinning site with a spacing 4d. Such lines were stacked in the vertical direction in such a way that adjacent lines were displaced relative to each other in the horizontal direction by distance 2d [a centered (C) (4 × 2) structure]. In this case, vortices formed a slightly deformed (1:1.12) triangular lattice. At $H_{1/2}$, vortices occupied every other pinning site in both horizontal and vertical directions, forming a C(2 × 2) square lattice (Fig. 1B). At n = 1, vortices occupied all of the pinning sites without any vacancies or interstices (Fig. 1C).

When $H > H_1$, vortices began to squeeze themselves at interstitial points as "quasi-bound" (*16*) or "caged" (*17, 18*) vortices. These points were the most stable places for additional vortices to penetrate a square array of vortices that were strongly pinned by defects. In the case of a pit with a larger radius than the penetration depth, two or more vortices would be trapped at a single defect (*9*).

Interstitial vortices were observed to be randomly distributed until H reached $H_{3/2}$, when additional vortices entered every other interstice, thus occupying just half of the interstitial sites (Fig. 1D). Between H_1 and $H_{3/2}$, the interaction of distant interstitial vortices was too weak to form a regular lattice. Even for $H_{3/2}$, the interstitial vortex that should be situated at the top left portion of the micrograph is mislocated at the interstitial position one line lower (Fig. 1D). At $H = H_2$, all of the interstitial sites were occupied by vortices, forming a C(1 × 1) square lattice (Fig. 1E).

At $H = H_{5/2}$, additional vortices entered every other interstice of the configuration at H_2, thus forming a C(2 × 2) square lattice (Fig. 1F). The two interstitial vortices did not overlap but were situated side by side, separated by a distance of ~0.6d. They were aligned parallel to one of the square edges. In the present case, the directions of the two vortices were accidentally horizontal. One vortex and two vortices alternately occupied the interstitial sites.

When H reached H_3, two vortices were located at every interstitial site (Fig. 1G). The direction of these two interstitial vortices switched alternately from horizontal to vertical. When $H = H_4$, all of the pairs of squeezed vortices were situated at every interstice and were aligned in the vertical direction (Fig. 1H). Additionally, a vortex was inserted at every middle point between two adjacent sites in the vertical direction (Fig. 1H). As a result, vortices formed a C(1 × 1/2) lattice.

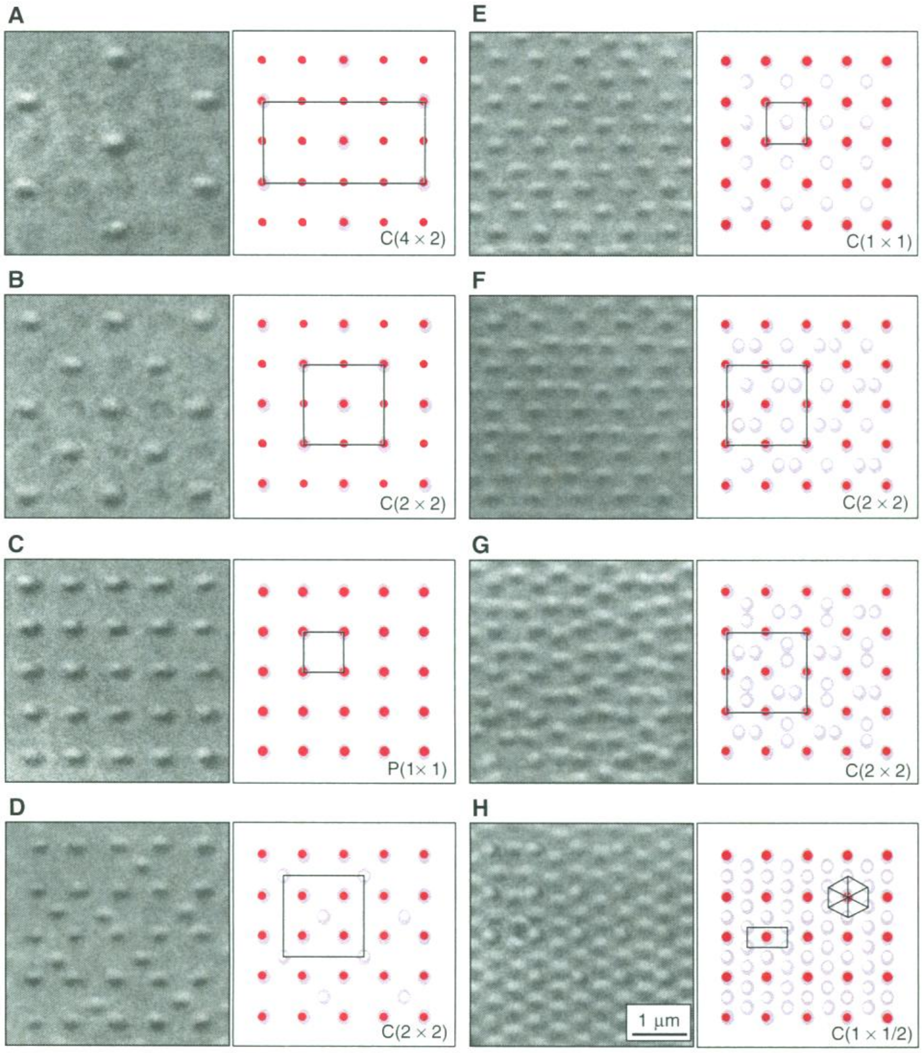

Fig. 1. Lorentz micrographs and schematics of the vortex configuration in a square array of artificial defects at matching magnetic fields H_n: (**A**) n = 1/4, (**B**) n = 1/2, (**C**) n = 1, (**D**) n = 3/2, (**E**) n = 2, (**F**) n = 5/2, (**G**) n = 3, and (**H**) n = 4. Red dots and blue open circles in each schematic show the defects and the vortices, respectively. Gray squares also indicate unit cells of the vortex lattices in each case. Vortices form regular lattices at the matching magnetic field H_1, as well as at its multiples and its fractions.

Vortices form regular lattices and consequently the most stable configurations at H_n. Therefore, the vortices do not move easily. Especially for $n = 1$, all of the defects are occupied by vortices and therefore hopping of vortices is forbidden even when the elementary force is exerted on them. In this case, the Mott-insulator phase, introduced by Nelson and Vinokur (19) and by Blatter *et al.* (20), is realized. In contrast, interstitial vortices, appearing at $H > H_1$, cannot be localized by much shallower pinning potentials at interstices. As a result, interstitial vortices demonstrate a "metallic" vortex behavior. Both localized vortices at defects and metallic vortices at interstices can be more directly observed by monitoring of their dynamics.

Peaks and cusps in J_c and M were found at $H = H_{1/4}$ and $H_{1/2}$ but not at $H_{3/2}$ or $H_{5/2}$ by macroscopic measurements (6). This is reasonable because the pinning potential at defects ($n < 1$) is deeper than that at interstices ($n > 1$). In fact, the regular lattice was partially destroyed at $H = H_{3/2}$ or $H_{5/2}$, even in the field of view shown in Fig. 1, D and F.

The dynamic behavior of vortices was then observed when H changed. The sample was first cooled down to 4.5 K and H was gradually increased. At a few Gauss, vortices began to penetrate the film from the film edge. They approached the defect region and soon occupied the front row of defects (Fig. 2A). Subsequent vortices approached this line barrier but could not easily get over it. When the vortices finally broke through the line, they jumped to defects as far away as 5*d* or more (21). When distant defects were occupied, vortices began to jump to nearer defects.

When all of the defects were occupied by vortices, new vortices accumulated in front of the first row because they could not enter the defect region. Before long, however, they began to enter interstices (Fig. 2B). The vortices continued to hop from one interstice to another. In Fig. 2C, the positions of interstitial vortices are displaced downward from their proper positions because of the force in the downward direction.

The manner of the vortex flow changed after all of the interstices were occupied. Without any vacant sites to hop to, they began flowing simultaneously in single lines. A few lines of flow in the field of view are shown in Fig. 2D.

When H was decreased, a force was exerted in the opposite direction and interstitial vortices began to leave the film. Vortices were displaced upward from the proper interstitial position because of this force (Fig. 2E). Even when vortices outside the defect region disappeared, vortices forming a square lattice resisted moving (Fig. 2F).

When H was further decreased, vortices began to depin. For example, one vortex in the front row was depinned and then a vortex in the second row hopped to the vacant site to form a hole (shown as h in Fig. 2G). In the meantime, opposite vortices (antivortices) began to enter and be trapped (o in Fig. 2G).

The above experiments showed that the character of the vortex flow somehow changed every time when the vortices formed closely packed regular lattices. Consequently, this indicates that the pinning force of a whole vortex lattice can change at H_n.

Peaks in J_c could more directly be explained by the different dynamic behaviors of vortices in two cases in which H is exactly H_1 and H is slightly greater than H_1. In the sample that was field-cooled down to 4.5 K at $H = 31$ G, just above H_1 (29.8 G), the interstitial vortex marked in red in Fig. 3A began to hop in the downward direction when H was increased to 39 G. When T was increased to 7 K to shorten the time-scale of the vortex hopping due to thermal fluctuations, the interstitial vortex hopped to the next interstitial site (Fig. 3B). (This micrograph was taken after the sample had been cooled down to 4.5 K, in order to obtain a high-contrast vortex image, but we confirmed that this cooling procedure did not change the configuration of the vortices.) When T was further increased to 7.5 K, the vortex hopped to the next site again (Fig. 3C). The interstitial vortex hopping from one site to another reminded us of the hopping conductivity of charge carriers in donor-doped semiconductors.

Excess vortices in a regular vortex lattice were observed to hop easily [see also flux flow results in (18)], whereas a change in magnetic field two times larger was required to induce hopping of the vortices forming the lattice. We also observed the hopping of "holes" in a vortex lattice. A stronger force was needed to cause a vortex hole to hop than to cause an excess vortex to do so, because a vortex must be depinned from a stable defect site. Similar vortex behavior was detected at other matching fields, such as H_2 and H_3, although it was not as conspicuous as in the case of $H = H_1$.

These studies elucidate the microscopic mechanism of the matching effects. When vortices formed a regular lattice, they could not begin to move unless a force larger than the elementary pinning force was exerted. At the same time, excess (or deficient) vortices were observed to move easily when affected by the Lorentz force,

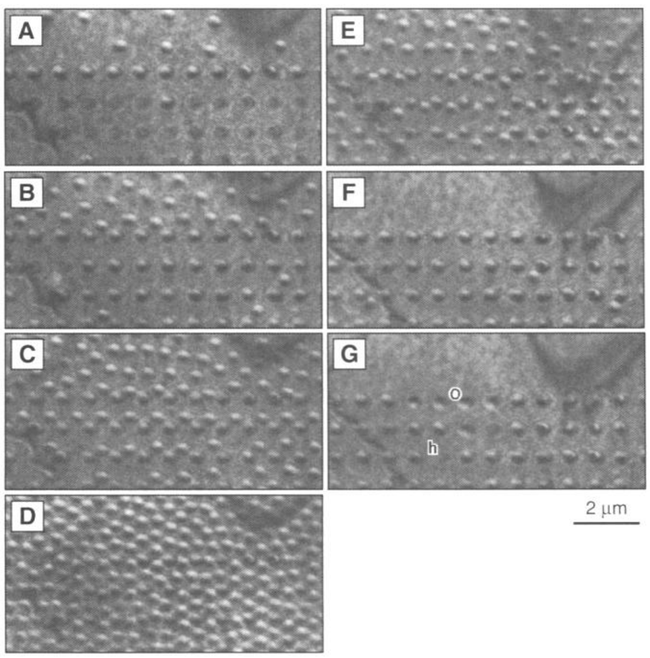

Fig. 2. Lorentz micrographs demonstrating the dynamic behavior of vortices when H is increased and then decreased gradually ($T = 4.5$ K); see text. The fields, in units of H_1; were (**A**) 0.2, (**B**) 0.5, (**C**) 1.2, (**D**) 2.5, (**E**) 1.5, (**F**) 0.9, and (**G**) 0.6. Video clips showing the movement of the vortices under similar conditions are available at http://www.sciencemag.org/science/feature/data/harada.shl.

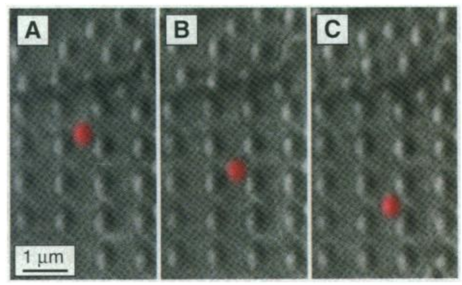

Fig. 3. Dynamics of an excess vortex. The excess vortex (red) hopped from one interstitial site when H changed from 31 to 39 G and T increased from (**A**) 4.5 K to (**B**) 7 K and then to (**C**) 7.5 K.

thus providing a microscopic explanation for the large critical current at matching magnetic fields.

REFERENCES AND NOTES

1. K. E. Osborne, *Philos. Magn.* **23**, 1113 (1971).
2. A. F. Mebard *et al.*, *IEEE Trans. Magn.* **1**, 589 (1977).
3. A. N. Lykov, *Solid State Commun.* **86**, 531 (1993).
4. V. V. Moshchalkov *et al.*, *Jpn. J. Appl. Phys.* **34**, 4459 (1995).
5. M. Baert *et al.*, *Phys. Rev. Lett.* **74**, 3269 (1995).
6. V. V. Metlushko *et al.*, *Solid State Commun.* **91**, 331 (1994).
7. C. P. Herring, *Phys. Lett.* **47A**, 105 (1974).
8. H. Dai *et al.*, *Science* **265**, 1552 (1994).
9. A. Bezryadin and B. Pannetier, *J. Low Temp. Phys.* **102**, 73 (1996).
10. S. Behler *et al.*, *Phys. Rev. Lett.* **72**, 1750 (1994).
11. L. N. Vu *et al.*, *Appl. Phys. Lett.* **63**, 1693 (1993).
12. K. Harada *et al.*, *Nature* **360**, 51 (1992).
13. J. E. Bonevich *et al.*, *Phys. Rev. Lett.* **70**, 2952 (1993).
14. T. Matsuda *et al.*, *Science* **271**, 1393 (1996).
15. K. Harada *et al.*, *Phys. Rev. B* **53**, 9400 (1996).
16. I. B. Khalfin and B. Ya. Shapiro, *Physica C* **207**, 359 (1993).
17. L. Radzihovsky, *Phys. Rev. Lett.* **74**, 4923 (1995).
18. E. Rosseel *et al.*, *Phys. Rev. B* **53**, R2983 (1996).
19. D. R. Nelson and V. M. Vinokur, *ibid.* **48**, 13060 (1993).
20. G. Blatter *et al.*, *Rev. Mod. Phys.* **66**, 1125 (1994).
21. It was pointed out by E. Zeldov that vortices were driven toward the center of the defect region by the force that was due to the Meissner current [E. Zeldov *et al.*, *Phys. Rev. Lett.* **73**, 1428 (1994)].

22. We thank N. Osakabe, T. Onogi, and R. Sugano of the Advanced Research Laboratory, Hitachi, Ltd., for discussions and comments; H. Hirose, H. Koike, and T. Ohnishi of the Instrument Division, Hitachi, and T. Kamino of Hitachi Instrument Engineering for assistance in operating the focused ion beam machine; F. Nagata and T. Shimotsu of Hitachi Instrument Engineering for discussion and electron microscopic observation; and S. Kubota, S. Matsunami, and N. Moriya of the Advanced Research Laboratory, Hitachi, for technical assistance in the experiment. V.V.M. acknowledges support from the Belgium Concerted Action (GOA) and National Fund for Scientific Research (NFWO) programs.

4 June 1996; accepted 6 September 1996

Human Influence on the Atmospheric Vertical Temperature Structure: Detection and Observations

Simon F. B. Tett,* John F. B. Mitchell, David E. Parker, Myles R. Allen

Recent work suggests a discernible human influence on climate. This finding is supported, with less restrictive assumptions than those used in earlier studies, by a 1961 through 1995 data set of radiosonde observations and by ensembles of coupled atmosphere-ocean simulations forced with changes in greenhouse gases, tropospheric sulfate aerosols, and stratospheric ozone. On balance, agreement between the simulations and observations is best for a combination of greenhouse gas, aerosol, and ozone forcing. The uncertainties remaining are due to imperfect knowledge of radiative forcing, natural climate variability, and errors in observations and model response.

There is considerable interest in the detection of a human influence on climate (*1*). Recent studies (*2, 3*) have suggested that anthropogenic changes in greenhouse gases, sulfate aerosols, and stratospheric ozone (O_3) may have altered the vertical temperature structure of the atmosphere. In (*2*), simulations from several climate models were used to show that the pattern similarity between modeled and observed changes increased from 1963 to 1987. Several assumptions were made by Santer *et al.* (*2*): that the response to stratospheric O_3 changes can be added linearly to other responses, that the response of sea surface temperatures and clouds to O_3 changes can be ignored (*4*), that the lags between radiative forcing and climate response can be ignored, and that the response to forcings from different periods can be combined linearly.

We avoided making these assumptions by using time-dependent simulations from a single model including all the forcings. We extended the analysis to include the effect of the spatial mean as well as the patterns of change, and we extended the period considered to 1961 through 1995 by using a new radiosonde temperature data set. With less restrictive assumptions than those used in (*2*), we confirm that recent climate changes are unlikely to be entirely due to unforced climate variability. We show that our model is, on balance, in best agreement with the patterns and spatial means of recent climate change over this extended period when forced with a combination of increases in greenhouse gases and tropospheric sulfate aerosols, and stratospheric ozone loss.

Our model, HADCM2 (*5*), is a coupled atmosphere-ocean model with all components (ocean, atmosphere, and ice and land surface) having a horizontal resolution of 2.5° in latitude by 3.75° in longitude. The atmosphere has 19 levels, with 5 levels above 100 hPa, and the ocean has 20. Atmospheric temperature data were diagnosed on 15 pressure levels (*6*). To assess the significance of our results, we used data from 700 years of a control integration of HADCM2 where climate forcing was kept constant (*7*). The standard deviation (SD) of annual mean tropospheric temperature in this control simulation is similar to that observed (*7*), which gives some confidence in model estimates of natural variability.

Three different climate forcings (G, GS, and GSO) were used to force HADCM2. To reduce noise, we computed the responses to each forcing by averaging the responses from an ensemble of four simulations. Responses are identified by the name of the forcing used. The G and GS simulations were started from four states in the control integration separated by 150 years (*8*).

In G, HADCM2 was forced with an increase in equivalent CO_2, representing the effect of observed changes in all greenhouse gases, including CO_2, methane, and chlorofluorocarbons from 1860 to 1996 (*5, 9*). In GS, HADCM2 was forced, in addition, with a simple parameterization of the effects of

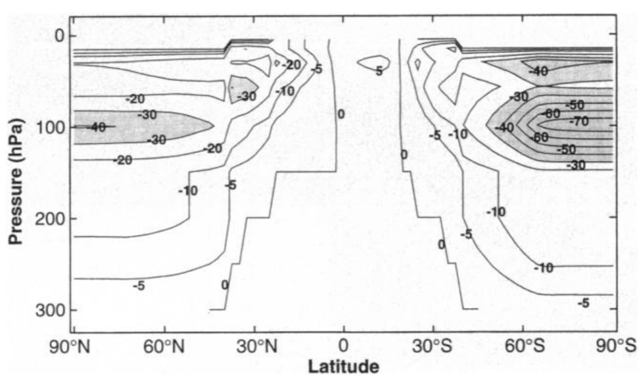

Fig. 1. Annual mean mass mixing ratio O_3 trends ($\times 10^9$) per year based on the use of a contour interval of 10×10^{-9} per year with extra contours at $\pm 5 \times 10^{-9}$ per year. Stippling shows where values are less than -30×10^{-9} per year.

S. F. B. Tett, J. F. B. Mitchell, D. E. Parker, Hadley Centre for Climate Prediction and Research, UK Meterological Office, London Road, Bracknell, Berkshire RG12 2SY, UK.
M. R. Allen, Space Science Department, Rutherford Appleton Laboratory, Chilton, Didcot, OX11 0QX, UK.

*To whom correspondence should be addressed. E-mail: sfbtett@meto.gov.uk